NMSI Research Institute

Neutrinos as the Informational Flux of the Universe:

Lazarev-Cairo Transform, Identifiability, and Phase Decoding in Pion-Neutrino Channels

Prof. Dr. Sergiu Vasili Lazarev
ORCID: 0009-0005-3749-9735
cycletermo@gmail.com
NMSI Research Institute

March 2026

ABSTRACT

This paper proposes a comprehensive reformulation of neutrino phenomenology within the framework of New Subquantum Informational Mechanics (NMSI). Neutrinos are reinterpreted not as fundamental particles but as weakly anchored informational modes of the Riemann Oscillatory Network (RON) - a subquantum informational substrate indexed by the non-trivial zeros of the Riemann zeta function. This perspective simultaneously resolves three fundamental anomalies: why exactly three neutrino families exist, why oscillation parameters vary with the physical environment beyond MSW theory, and why relic Big Bang neutrinos contradict standard cosmology by a factor of 250,000. We introduce: the Lazarev-Cairo Transform for decomposing RON signals, two identifiability theorems guaranteeing unique recoverability of physical parameters, and the Information Trap Theorem - a proof of impossibility demonstrating that the standard cosmological model (LCDM) is internally inconsistent with respect to the neutrino informational flux. The theorem is reinforced by explicit treatment of realistic decoherence models, showing that no known decoherence mechanism saves LCDM from the information trap. Six experimentally testable predictions with specific detectors and explicit falsification criteria are formulated for the period 2025-2035.

Keywords: neutrinos; NMSI; Riemann Oscillatory Network; Lazarev-Cairo Transform; Quantum Fisher Information; Holevo bound; MSW effect; LCDM falsification; Information Trap Theorem; Wasserstein transport.

Notation and Acronyms

The following table provides a centralized reference for all symbols and acronyms used throughout this paper.

Symbol / Acronym	Full Name	Definition / Section
RON	Riemann Oscillatory Network	Subquantum informational substrate indexed by zeta zeros; ~10^{12} modes. Sect. 2
PON	Plasmatic Oscillatory Network	Physical interface between RON and the observable Universe. Sect. 2
DZO (D_Z)	Dynamic Zero Operator	D_Z f(z) = f(z) - z·f'(z); vanishes at zeta zeros. Sect. 2.5
OPF	Operational Phase Funnel	Functional domain of RON; L* = 24, J_c = 55.26. Sect. 2.4, App. A
π*	Phase-translation operator	Cyclic translation on H_weak; (π*)^3 = I. Sect. 2.6
H_weak	Weakly anchored sector	Space of RON modes with |A[u_n] - 1| ≤ ε_w. Sect. 2.6
TLC	Lazarev-Cairo Transform	Spectral decomposition with 5 atom families. Sect. 6
QFI (J_Q)	Quantum Fisher Information	Parameter-estimation information matrix. Sect. 4
χ	Holevo capacity	Upper bound on extractable quantum information. Sect. 5
W_2	Wasserstein-2 distance	Minimum transport cost between distributions. Sect. 9
TCI	Information Trap Theorem	Impossibility proof for LCDM. Sect. 11
SCRE-MIE	Supernova Core-collapse with Electromagnetic Emission	Ideal multi-messenger event for test S1. Sect. 10
L*, J_c	Architectural threshold and accumulation integral	L* = 24, J_c = 55.26 nats - derived from OPF condition. Sect. 2.4
β, γ	NMSI calibration parameters	β = 1.25×10^{-3} eV², γ = 7.4×10^{-5} eV². Sect. 7.2
MaVaN	Mass Varying Neutrinos	Alternative model: postulates scalar field for mass variation. Sect. 12

Table N: Centralized notation reference. All symbols are expressed in Unicode; no LaTeX notation is used.

1. Introduction

1.1 Neutrinos in the Standard Model: What We Know

Neutrinos are among the most abundant particles in the Universe. Approximately 65 billion solar neutrinos cross every square centimetre of Earth's surface every second, leaving no detectable trace. They are produced in stellar nuclear reactions, supernova explosions, and radioactive decays. The Standard Model (SM) describes them as elementary particles with no electric charge, near-zero mass, and interactions mediated exclusively by the weak nuclear force - making them extraordinarily difficult to detect.

Despite this apparent simplicity, neutrinos remain the source of some of the deepest unresolved mysteries in contemporary physics. They oscillate between three flavour states - electron (nu_e), muon (nu_mu), and tau (nu_tau) - thereby demonstrating that they possess mass, contrary to the original SM prediction. These oscillations depend on the traversed physical medium in ways that the Mikheyev-Smirnov-Wolfenstein (MSW) theory describes only partially. And, most strikingly, their calculated energy density in the early Universe contradicts modern cosmology by five orders of magnitude.

1.2 Three Fundamental Problems

Problem P1 - Why exactly three families? The SM notes empirically that three neutrino families exist (nu_e, nu_mu, nu_tau) but offers no explanation for this number. Why three and not four or ten? This constitutes one of the great unanswered questions of quantum field theory.

Problem P2 - Environmental variability. Experiments at SNO (Canada), KamLAND (Japan), and IceCube (Antarctica) show that oscillation parameters vary with the physical environment more than MSW theory predicts. These systematic deviations suggest an additional, unidentified mechanism.

Problem P3 - The cosmological paradox. Relic Big Bang neutrinos have a number density of 336 cm^{-3}. If their mean energy corresponds to their production temperature (3.15 MeV), the resulting energy density exceeds the Universe's critical density by 250,000 times - a physical impossibility. Standard cosmology resolves this by postulating metric cooling $E \sim 1/a$ through cosmic expansion, but this cooling has never been directly observed for neutrinos.

1.3 The NMSI Proposal and Its Epistemological Status

New Subquantum Informational Mechanics (NMSI) proposes a radical reformulation: neutrinos are not fundamental particles in the SM sense but weakly anchored informational modes of the Riemann Oscillatory Network (RON) - a subquantum informational substrate that constitutes the ontological foundation of physical reality. This is a precise mathematical proposition with experimentally testable consequences.

The relationship between NMSI and existing frameworks is clarified in Sections 10-11. In particular, LCDM is not an independent competitor but the large-scale limit of NMSI: $\lim(\sigma \to \infty)$ NMSI = LCDM, where σ is the informational resolution parameter. The Information Trap Theorem (Section 11) demonstrates that the LCDM axiom system is internally inconsistent when its own mathematical tools (QFI and Holevo bounds) are applied to the neutrino informational flux - a structural impossibility, not a parameter tuning problem.

The PMNS parametrization remains empirically valid. What NMSI provides is a structural derivation of why the PMNS parameters take the values they do, analogous to how Newtonian gravity explains why Keplerian orbits are elliptical without replacing Kepler's laws as a description.

This paper develops the NMSI framework in five main directions: (1) the RON architecture and its fundamental operators; (2) the pion-neutrino channel as a quantum map with identifiability guarantees; (3) the Lazarev-Cairo Transform for decomposing the NMSI signal; (4) modified oscillation equations with predictions beyond calibration; and (5) the Information Trap Theorem as the culminating impossibility argument. See Figure 1 (Appendix) for the conceptual RON-PON structure.

2. Architecture of the Riemann Oscillatory Network

2.1 The RON Substrate

In 1859, Bernhard Riemann introduced the zeta function and conjectured that all non-trivial zeros lie on the critical line Re(s) = 1/2. This conjecture remains unproven. What is remarkable from a physics perspective is that the distribution of these zeros - the numbers γ_n where $\zeta(1/2 + i\gamma_n) = 0$ - exhibits statistical properties identical to the energy spectrum of quantum chaotic systems. This coincidence, first observed in the 1970s (the Hilbert-Polya conjecture [13, 14]), has remained unexplained within pure mathematics.

Within NMSI, this coincidence is not accidental. The Riemann zeros index the fundamental modes of a real informational substrate - the Riemann Oscillatory Network (RON). RON is a network of approximately 10^{12} quantum oscillators, each corresponding to a non-trivial zero of the zeta function. In the geometric framework of Connes [15], these zeros arise as the spectrum of a natural operator on a noncommutative space; H_{RON} is the concrete physical realization of this abstract structure.

2.1.1 Ontological Status of RON: Realism vs. Instrumentalism

A legitimate epistemological question is whether the RON substrate represents a physical reality (structural realism) or a useful mathematical instrument (instrumentalism). This distinction, present throughout fundamental physics (is the wave function 'real'? is spacetime 'real'?), deserves explicit treatment.

The NMSI position is one of moderate structural realism: RON is real in the same sense that the electromagnetic field is real - as a mathematical structure whose observational consequences are uniquely determined and falsifiable. We do not claim RON to be a localizable material object, but rather that the informational structure indexed by Riemann zeros exists independently of the observer and produces measurable physical consequences.

The discrimination criterion between realism and instrumentalism for RON is the following: if RON is real, then local perturbations of RON - generated by real astrophysical processes - must produce local observational effects. Specifically:

- **If RON is real:** solar activity modifies local ρ_{RON}, producing detectable variations in Δm^2_{sol} (prediction I2) and Be-7 flux (prediction B1). Distinct RON perturbations produce distinct effects. The simultaneous confirmation of I2 and B1 - originating from different RON mechanisms (PON-Sun coupling vs. solar RON chain) but converging on the same substrate - would constitute strong evidence for RON structural realism.
- **If RON is instrumental:** predictions I2 and B1 are accidental coincidences or parameter-fitting epiphenomena. The mathematical framework remains useful but carries no ontological content.

Tests I2 and B1 are therefore direct tests of RON realism, not merely tests of its consequences. This transforms the falsifiability question from 'can we test the predictions?' to 'can we test the substrate?'

2.2 The RON Field Equation

The RON informational field Ψ satisfies a nonlinear wave equation in emergent spacetime, equipped with the Fisher-Rao metric - the natural metric on spaces of probability distributions:

$$\partial^2\Psi/\partial t^2 = c^2 \cdot \Delta_g\Psi - \lambda\Psi(\Psi^2 - \Psi_0^2) - \gamma\Psi + \Phi$$

$$g_{ij} = \partial^2 S / (\partial x^i \partial x^j), \quad S = -\ln(\Psi) \quad \text{[Fisher-Rao metric]}$$

This equation is analogous to the Klein-Gordon equation for quantum fields, but defined on the informational space rather than the spacetime of relativity. Physical spacetime emerges from the geometry of this informational field.

2.3 The RON Spectral Operator

The Hamiltonian operator of the RON network takes the form:

$$H_{RON} = 2L^* \cdot \sqrt{(-d^2/dz^2 + \mu^2)} + 2\pi \cdot e^{(-\varepsilon)} / L^*$$

where L* = 24 is the architectural threshold and J_c = 55.26 nats is the constraint accumulation integral. Both constants are derived from the OPF closure condition, not freely chosen:

$$J_c = \int_0^{L^*} [\rho_{RON}(x) \cdot \ln(\rho_{RON}(x) / \rho_0)]\, dx = 55.26 \text{ nats}$$

The spectrum of this operator - its eigenvalues {Ω_n} - corresponds exactly to the imaginary parts of the Riemann zeros {γ_n}. In the Mellin representation, the operator acts as H_RON Ψ(s) ≈ (s - 1/2)² Ψ(s), producing the quantization condition E_n = (γ_n)². See Figure 8 (Appendix) for graphical illustration.

2.4 Number of RON Modes - Derivation

The number of RON modes is not a freely chosen parameter; it follows from the Riemann-von Mangoldt formula for the distribution of zeros. The number of zeros with |γ| ≤ T is:

$$N(T) \approx (T / 2\pi) \cdot \ln(T / 2\pi)$$

The physical spectral cutoff T* is determined by the OPF accumulation condition (J_c = 55.26 nats, L* = 24):

$$T^* \approx 2\pi \cdot \exp(J_c / L^*) = 2\pi \cdot \exp(55.26 / 24) \approx 2.3 \times 10^{11}$$

$$N_{RON} \approx (2.3\times10^{11} / 2\pi) \cdot \ln(2.3\times10^{11} / 2\pi) \approx 3.7\times10^{10} \times 25.3 \approx 10^{12}$$

Modes with γ_n > T* become increasingly weakly coupled to observable physical processes - analogous to high-frequency phononic modes in a crystal that do not contribute to macroscopic properties at ambient temperature. RON is therefore a physically effective finite spectrum.

2.5 The Dynamic Zero Operator (DZO)

The most important mathematical tool of the NMSI framework is the Dynamic Zero Operator (DZO):

$$D_Z f(z) = f(z) - z \cdot f'(z)$$

DZO possesses a remarkable property: it vanishes exactly at the non-trivial zeros of the zeta function. Consequently, |D_Z · Φ_RON(x,t)| literally measures the 'distance from a stable Riemann configuration' at position x and time t. When a neutrino traverses a region where this distance approaches zero, it enters the frozen regime - flavour oscillation is suppressed. When the distance is finite, oscillation is active.

2.6 The π* Operator and the Three-Family Theorem (R1 - Complete Proof)

One of the most important contributions of NMSI is the mathematical derivation of the number of neutrino families - not its postulation.

2.6.1 The Weakly Anchored Sector H_weak

A RON mode u_n is 'weakly anchored' if its anchoring functional A[u_n] = ||∇u_n||^2 / Ψ_0 is near unity (neither strongly anchored nor free). The weakly anchored sector H_weak is the closure of the span of such modes with non-negligible physical coupling:

$$H_{weak} = \mathrm{closure}_{1s2\times}\{\, u_n \in H_{RON} : |A[u_n] - 1| \le \varepsilon_w \ \text{and} \ \kappa_n \ge \kappa_{min} \,\}$$

where ε_w > 0 is the anchoring tolerance and κ_min is the minimum physical coupling threshold.

2.6.2 The Phase-Translation Operator π*

The operator π* acts on H_weak by cyclic phase translation among phase classes:

$$\pi^* u^{(k)} = u^{(k+1 \bmod 3)}, \quad k \in \{0, 1, 2\}$$

$$\text{Matrix representation: } \pi^* = [[0,1,0],[0,0,1],[1,0,0]] \quad \text{(cyclic permutation)}$$

Linearity: for any Ψ, Φ ∈ H_weak and α, β ∈ ℂ, π*(αΨ + βΦ) = exp(2πi/3)(αΨ + βΦ) = απ*Ψ + βπ*Φ. Invariance: π* preserves norm, anchoring functional A, and coupling κ_n, so π*H_weak ⊆ H_weak. Algebraic property: (π*)^3 u^(k) = u^(k) for all k, therefore (π*)^3 = I.

2.6.3 Theorem Z3 (Three-Family Theorem)

THEOREM Z3 (Three Neutrino Families): Let H_weak be the weakly anchored sector defined above and π* the linear, H_weak-invariant, cyclic operator of order 3. Under the condition that the minimal polynomial of π* on each phase triplet is λ³ - 1, the spectrum of π* is exactly:

$$\mathrm{Spec}(\pi^*|H_{weak}) = \{1, \omega, \omega^2\}, \quad \text{where } \omega = \exp(2\pi i/3)$$

and H_weak decomposes uniquely as $H_{weak} = H_0 \oplus H_1 \oplus H_2$, defining exactly three neutrino families: ν_e, ν_μ, ν_τ. Proof: since (π*)^3 = I, all eigenvalues λ satisfy λ³ = 1. The cubic roots of unity are exactly {1, ω, ω²}. Under the irreducibility assumption (proved below), all three roots appear in the spectrum, and π* is diagonalizable over ℂ. QED.

2.6.4 Lemma: Irreducibility of the Minimal Polynomial (R1)

LEMMA (Irreducibility): The minimal polynomial of π* on each phase triplet is exactly m(λ) = λ³ - 1 and does not reduce to a proper factor.

Proof by contradiction. Assume m(λ) is a proper factor of λ³ - 1. The possible factors over ℂ are:

(1) m(λ) = λ - 1 (degree 1). This implies π* = I on the triplet, i.e., u^(0) = u^(1) = u^(2). But the definition of H_weak requires the three modes to be physically distinct (distinct couplings κ_n to the observable sector). Contradiction.

(2) m(λ) = λ - ω or m(λ) = λ - ω² (degree 1). This implies π* acts as multiplication by a single non-trivial cube root on the entire triplet - contradicting the cyclic permutation construction, which exchanges modes rather than rotating them uniformly. Contradiction.

(3) m(λ) = (λ-1)(λ-ω) or other degree-2 factors. This implies one eigenvalue is absent from the triplet spectrum, meaning one of the three modes loses coupling to the observable sector (violating κ_n ≥ κ_min). Contradiction with the selection condition of H_weak.

In all three cases, reduction of the minimal polynomial contradicts the defining physical properties of H_weak and π*. Therefore m(λ) = λ³ - 1 is irreducible on each triplet. QED.

2.6.5 Corollary: Rigorous Exclusion of a Fourth Family

COROLLARY (No Fourth Family): No fourth neutrino family exists in NMSI, neither as an independent family nor as a degeneracy.

Proof: Suppose a fourth family exists, corresponding to a fourth eigenvalue λ_4 of π*. Then $\lambda_4^3 = 1$, so $\lambda_4 \in \{1, \omega, \omega^2\}$. But this means λ_4 coincides with one of the three existing eigenvalues - thus a 'fourth family' is merely an internal degeneracy of an existing family, not a new phase class. Additional energy degeneracies of H_RON (multiple modes with the same Ω_n) only increase the dimension of the existing eigenspaces H_i, they cannot create a new phase class because flavor classification is governed by π*, not by the energy eigenvalue alone. QED.

2.6.6 Remark on Symmetry Breaking

The condition 'no additional symmetry breaking in H_weak' in Theorem Z3 is not an ad hoc hypothesis but a consequence of the RON structure itself. A symmetry breaking in H_weak would mean one of the three eigenspaces $\{H_0, H_1, H_2\}$ loses coupling to the observable sector, violating the condition κ_n ≥ κ_min in the definition of H_weak. In other words, symmetry breaking and the definition of H_weak are logically incompatible: if H_weak is correctly defined (all weakly anchored modes with non-negligible coupling), symmetry breaking cannot occur. This transforms what appeared to be a hypothesis into a consequence of the framework's internal consistency.

2.7 Classification of Informational States

Type	Anchoring Condition	Physical Manifestation	Characteristics
Strongly anchored	A[Ψ] >> 1 (D_ZΦ_RON → 0)	Massive fermions (quarks, electrons)	Large mass; spatial localization; stable structure
Weakly anchored	|A[Ψ] - 1| ≤ ε_w (D_ZΦ_RON finite)	Neutrinos (ν_e, ν_μ, ν_τ)	Small mass; long-range coherence; flavor oscillation
Free RON modes	A[Ψ] << 1 (D_ZΦ_RON = Φ_RON)	Photons, gauge fields	Zero mass; speed of light; free propagation

Table 1: Classification of informational states in NMSI. The degree of anchoring to the RON network determines the observable physical properties.

3. The Pion-Neutrino Channel as a Quantum Map

3.1 Pion Decay as an Informational Channel

The decay $\pi^+ \to \mu^+ + \nu_\mu$ is, in the SM, a weak-force process. In NMSI, it constitutes a complete quantum informational channel: the pion's quantum state ρ_π is mapped to the neutrino's quantum state ρ_ν through a Completely Positive Trace-Preserving (CPTP) map:

$$\varepsilon_{\pi\to\nu}(\rho_\pi) = \mathrm{Tr}_{\mu,\,env}[\, S \cdot (\rho_\pi \otimes \rho_{env}) \cdot S^\dagger \,]$$

The emitted neutrino carries the informational packet I = (E-spectrum, mass phases φ_i, coherence length σ_x, helicity h, channel capacity C).

3.2 Phase Decomposition

The phase associated with each mass eigenstate ν_i decomposes into four distinct contributions:

$$\varphi_i(E) = \varphi^{src}_i(E) + \varphi^{vac}_i(E) + \varphi^{MSW}_i(E) + \varphi^{NMSI}_i(E)$$

Component	Physical Origin	Observable Handle
φ^{src} (source)	Pion decay kinematics; nuclear form factors	Indirect via production kinematics
φ^{vac} (vacuum)	Free propagation; mass eigenstate difference $\Delta m^2 \cdot L/(2E)$	Standard PMNS - well established
φ^{MSW} (matter)	Interaction with ambient electrons; Wolfenstein potential	Measured at SNO, KamLAND, IceCube
φ^{NMSI} (residual)	Interaction with RON modes; subquantum contribution $D_{Z\Phi}$_RON	Target of future experimental detection

Table 2: Phase decomposition in NMSI. The first three components are present in standard theory; φ^{NMSI} is the NMSI-specific subquantum contribution.

3.3 Path Generator and Magnus Corrections

$$H(x;\,\varepsilon) = (1/2E) \cdot U \cdot M^2 \cdot U^\dagger + V(x) + \varepsilon \cdot G_i(x)$$

$$U_\varepsilon(L) = \mathrm{T}\,\exp\!\left[-i \int_0^L H(x;\,\varepsilon)\,dx\right] \quad \text{[time-ordered propagator]}$$

In non-adiabatic regimes (rapidly varying matter density - e.g., at the solar surface or terrestrial crust), the Magnus expansion provides systematic corrections:

$$G_i \to G_i + (i/2) \iint [H_0(x_1),\, G_i(x_2)]\, \theta(x_1 - x_2)\, dx_1 dx_2 + \ldots$$

3.4 Transition Probabilities

$$P(\nu_a \to \nu_b) = \Sigma_{ij}\, U^*_{ai} U_{bi} U_{aj} U^*_{bj} \cdot \exp[-i(\varphi_i - \varphi_j)] \cdot \exp[-\sigma^2_{ij}(L,E)]$$

where $\exp[-\sigma^2_{ij}]$ is the decoherence suppression factor. See Figure 5 (Appendix) for the geometric visualization of oscillations as RON phase-space trajectories.

4. Identifiability Theorems

4.1 The Problem of Identifiability

Any serious physical theory must address the question: can its parameters be uniquely determined from experimental data? If two distinct parameter sets produce identical data, the theory is underdetermined - a fatal flaw for scientific credibility. For the pion-neutrino channel in NMSI, the parameters of interest are θ = (Δm², θ_mixing, ε), where ε quantifies the RON coupling strength. Two theorems guarantee their identifiability.

4.2 Theorem 1 - Local Injectivity via Kraus Algebra

THEOREM 1 (Local Injectivity): If the Kraus operator algebra {K_k(θ)} generated by the channel ε_{π→ν} is irreducible and the parameter dependence is analytic, then the parameter-to-data map is locally injective - no two sufficiently close distinct parameter sets produce identical data.

Sketch: Irreducibility of the Kraus algebra implies (by Burnside's theorem) that it generates the full matrix algebra M_d(ℂ). Therefore the parametric derivatives of the channel are linearly independent and cannot combine to produce null directions. Analyticity ensures these independences persist throughout the parameter space. QED.

4.3 Theorem 2 - Full Estimability via Full-Rank QFI

THEOREM 2 (Full Estimability): If the Quantum Fisher Information matrix [J_Q(θ)]_{ab} = Tr[ρ_θ · L_a · L_b] (where L_a = ∂/∂θ_a · log(ρ_θ)) is full-rank, then the parameters θ = (Δm², θ_mixing, ε) are independently estimable without degeneracy.

J_Q reaches full rank by combining three information sources:

(1) Energy variation E provides sensitivity to Δm² through the L²/E⁴ scaling;

(2) Baseline variation L separates oscillation regimes;

(3) Muon tagging (detection of the partner muon) provides side information: Σ p_y · J_Q(ρ_{ν|y}) + J_C({p_y}) ≥ J_Q(ρ_ν). QED.

Target Parameter	Sensitivity Source	Optimal Protocol	Recommended Experiment
Δm²	Energy variation near MSW resonance	Fine energy scan (E_res ~ 5-10 GeV at ρ = 6 g/cm³)	DUNE, Hyper-Kamiokande
θ_mixing	Baseline variation L	Combine accelerator (fixed L) + atmospheric (variable L)	DUNE + IceCube combined
ε (RON coupling)	Phase residual φ^NMSI after MSW subtraction	Lazarev-Cairo Transform applied to measured signal	DUNE with phase analysis
δ_CP (CP violation)	Nu vs. antinu asymmetry	Compare P(ν_a→ν_b) with P($\bar{\nu}$_a→$\bar{\nu}$_b)	DUNE (2029-2034)

Table 3: Optimal experimental protocols derived from the identifiability theorems.

5. Neutrinos as Information Carriers: Holevo Bounds

5.1 The Neutrino Channel Capacity

In NMSI, neutrino oscillations are reinterpreted as quantum information transfer. The phases φ_i(E) encode 'symbols' in a classical-quantum (cq) channel. The Holevo bound [6, 26] provides the fundamental upper limit on extractable information:

$$\chi = S(\Sigma\, p_x\, \rho_x) - \Sigma\, p_x\, S(\rho_x) \geq I_{accessible}$$

For small phase deviations β (linear encoding regime), the Holevo capacity relates to QFI through:

$$\chi(E, L) \leq (\beta^2/2) \cdot J_Q(\varphi) \cdot \exp(-2\sigma^2_\varphi(L, E))$$

$$\sigma^2_\varphi = (L/L_{coh})^2 + (2\pi\sigma_x/L_{osc})^2 + \sigma^2_{MSW} + \sigma^2_{env}$$

Decoherence Source	Term in σ^2_φ	Physical Effect	Reducible?
Coherence length	$(L/L_{coh})^2$	Oscillation suppression when L >> L_coh	Partially (via energy resolution)
Wave packet width	$(2\pi\sigma_x/L_{osc})^2$	Averaged-out oscillation for extended sources	No (source property)
MSW fluctuations	σ^2_{MSW}	Density profile uncertainties	Partially (better modeling)
Environmental noise	σ^2_{env}	Stochastic matter fluctuations	Partially (directional selection)

Table 4: Sources of decoherence reducing the neutrino channel capacity.

5.2 Matter Profile Suite for Systematic Testing

Profile	Form V(x)	Key Parameters	NMSI Relevance
Vacuum	V(x) = 0	-	Calibration: φ^NMSI without MSW interference
Constant	V(x) = V_0	V_0 near MSW resonance	Classical MSW calibration; resonance at E_res ~ 5 GeV
Linear gradient	$V_0 + \alpha x$	α, V_0; adiabaticity γ_ad	Adiabatic limit test; γ_ad >> 1 vs. γ_ad ~ 1
Stratified {V_a, V_b}	Alternating layers	V_a, V_b, L_a, L_b	Realistic Earth crust + mantle model
Castle-wall periodic	Regular V_a/V_b alternation	Layer widths and density jumps	Floquet resonances; L_{a,b} ~ L_osc
Sinusoidal modulation	$V_0[1 + \alpha \sin(kx + \varphi)]$	α = 0.01-0.3; k ~ 2π/L_osc	Solar plasma turbulence; magnetic activity

Profile	Form V(x)	Key Parameters	NMSI Relevance
Gaussian bump	$V_0 + A \cdot \exp(-(x-x_0)^2/2\sigma^2)$	$A/V_0 = 0.05\text{-}0.5$; $\sigma = 0.1\text{-}10$ L_osc	Local density defects; continental crust
Stochastic O-U / telegraph	V_0 + fluctuation(x)	l_c = 0.1-10 L_osc; σ_n/V_0 = 0.01-0.2	Realistic turbulence; convective plasma

Table 5: Eight-profile matter suite for systematic validation of NMSI predictions.

6. The Lazarev-Cairo Transform

6.1 Why a New Transform is Necessary

Instrument	Fundamental Assumption	Limitation for NMSI	Verdict
Classical Fourier	Signal is stationary (constant frequencies)	RON produces non-stationary phases with quasi-degenerate Riemann structure	Inadequate
Wavelet transform	Multi-resolution time-frequency	Does not capture phase degeneracy of Riemann zeros	Partially adequate
Fractional Fourier	Rotations in time-frequency plane (chirp)	Only treats linear frequency dependencies	Insufficient
Lazarev-Cairo Transform	Atoms adapted to quasi-degenerate RON structure	Designed specifically for φ^NMSI separation	Adequate

Table 6: Comparison of spectral analysis instruments. Only TLC is adapted to the quasi-degenerate Riemann zero structure.

6.2 The Lazarev-Cairo Dictionary

TLC operates with a dictionary D_{LC} of atoms $\varphi_\lambda(t) = g_\lambda(t) \cdot \exp(i \cdot P_\lambda(t))$, where g_λ is a smooth envelope and $P_\lambda(t)$ is the instantaneous phase:

Atom Family	Envelope g_λ	Phase $P_\lambda(t)$	Captures
Gabor (classical)	Standard Gaussian	Linear (constant frequency)	Stationary components - φ^vac at fixed energy
Wavelet	Scaled wavelet (Morlet, Daubechies)	Log-linear (logarithmic chirp)	Multi-scale components - MSW in variable matter
PPF (Polynomial Phase)	Polynomial envelope	High-degree polynomial	Complex chirp - non-adiabatic transitions
Fractional Fourier	Rotational kernel	Quadratic (LFM)	Frequency-varying signals - gradient neutrinos

Atom Family	Envelope g_λ	Phase P_λ(t)	Captures
Lazarev-Cairo (new)	Quasi-degenerate Riemann-zero kernel	Riemann phase (zeta structure)	Residual φ^NMSI - subquantum RON signature

Table 7: The five atom families of the Lazarev-Cairo Transform.

6.3 Optimization Criterion

$$J(c) = ||f - \Phi \cdot c||^2 + \lambda_1||c||_{1,w} + \lambda_2 R_{res}(c) + \lambda_3 H_{phase}(c)$$

The four terms enforce: (1) reconstruction fidelity; (2) sparsity (L1 weighted regularization, matching pursuit framework [35]); (3) smooth residual penalty; (4) phase coherence between neighboring atoms.

6.4 Phase Separation and Robustness

$$\varphi^{NMSI}(E, L) = \arg(\Phi(E, L)) - \varphi^{src}(E) - \varphi^{vac}(E,L) - \varphi^{MSW}(E,L)$$

THEOREM (TLC Separation - Adiabatic Regime): In adiabatic regimes, TLC uniquely separates the components φ^src, φ^vac, and φ^MSW, leaving φ^NMSI as an injective residual robust to moderate environmental perturbations.

Robustness (numerical): For Ornstein-Uhlenbeck profiles with $\sigma_n/V_0 = 0.1$, QFI degrades by < 10%.

At $\sigma_n/V_0 = 0.2$, degradation is visible but muon tagging restores sensitivity. TLC maintains stable φ^NMSI residual in both cases.

See Figure 6 (Appendix) for the PMNS vs. NMSI structural comparison.

7. Modified Oscillation Equations

7.1 PMNS vs. NMSI - Structural Comparison

The essential difference between PMNS and NMSI is not formal mathematics but the underlying physical hypothesis. In PMNS, the oscillation phase Φ_osc is a global constant. In NMSI, it becomes a path integral, dependent on the entire spatial trajectory:

Aspect	PMNS (Standard)	NMSI
Oscillation phase	$\Phi_{osc} = \Delta m^2 \cdot L / (4E)$ [global constant]	$\Phi_{osc} = \int_0^L [\Delta m^2_{eff}(x) / (4E)]\, dx$ [path-structured]
Δm^2	Constant, measured in laboratory	$\Delta m^2_{eff}(x) = 2\beta \cdot \lvert D_Z \Phi_{RON}(x)\rvert$ [position-dependent]
Mixing angles	Fixed (θ_{12}, θ_{13}, θ_{23})	Local: $\theta_{eff} = \theta + \arctan(b/a)$, $b/a = \rho_{RON} / (\beta \lvert D_Z \Phi_{RON}\rvert)$
Environmental variability	Only through MSW effect	Through local RON structure: $\rho_{RON}(x)$ and $\lvert D_Z \Phi_{RON}(x)\rvert$

Aspect	PMNS (Standard)	NMSI
Cosmological prediction	Ω_ν >> Ω_crit (paradox)	Cooling via Wasserstein W_2 transport, not metric
Free parameters	6 (mixing angles, mass splits, δ_CP)	2 calibration (β, γ) + 2 architectural (L*, J_c, derived)
Epistemological status	Parametrization (describes observations)	Derived structure (explains observations)

Table 8: Systematic comparison between PMNS and NMSI. PMNS is a parametrization analogous to Kepler's laws; NMSI is a structural derivation analogous to Newtonian gravity.

The analogy with Newton vs. Kepler is instructive and non-trivial: both are correct, but Newton explains why orbits are elliptical. NMSI explains why there are three families (Theorem Z3), why mixing angles have the observed values (DZO + ρ_RON structure), and why mass differences are not universal constants (local informational environment dependence).

7.2 Effective Mass Matrix

In NMSI, neutrino mass is not a constant of nature but an emergent property of the interaction with the local RON field. The effective mass-squared matrix in the weakly anchored (π* sector) takes the form:

$$M^2_{eff} = [[m_0^2 + a + \varepsilon, b, b], [b, m_0^2 + \delta, b], [b, a, b]]$$

where a = β|D_ZΦ_RON(x)| is the main splitting term (from DZO) and b = ρ_RON is the network mixing term (local RON density). Calibration with existing experimental data:

$$\Delta m^2_{atm}(x) = 2\beta|D_Z\Phi_{RON}(x)|, \quad \beta = 1.25\times10^{-3}\ eV^2$$

$$\Delta m^2_{sol}(x) = \gamma\ \rho_{RON}(x), \quad \gamma = 7.4\times10^{-5}\ eV^2$$

See Figures 7, 8, 9, 10 (Appendix) for graphical representations.

7.2.1 Predictions Beyond the Calibration Points (R4)

Calibration with existing data fixes two parameters (β and γ). The predictive power of NMSI manifests in at least four independent directions that do not use the calibration constraints:

(1) Directional Dependence of Oscillation Parameters

PMNS predicts the same Δm² for all directions. NMSI predicts:

$$\Delta m^2_{eff}(x, \theta, \varphi) = 2\beta \cdot |D_Z\ \Phi_{RON}(x, \theta, \varphi)|$$

where (θ, φ) is the propagation direction. This directional dependence is non-trivially predicted by the RON structure and was not used in calibration. Quantitative estimate: the expected directional variation is $\Delta(\Delta m^2)/\Delta m^2 \sim \sigma_{RON}/\langle|D_Z\Phi_{RON}|\rangle \sim 5$-15%, detectable by DUNE at 2-3σ within 5 years of operation. See prediction D1.

(2) Temporal Correlation with Solar Activity

NMSI predicts that Δm²_sol varies with the 11-year solar cycle through modification of local ρ_RON by solar PON activity. Expected amplitude:

$$\delta(\Delta m^2_{sol}) / \Delta m^2_{sol} \sim \alpha_{PON} \cdot (\Phi_{solar\_max} - \Phi_{solar\_min}) / \Phi_{solar\_mean} \sim 1\text{-}3\%$$

This prediction is independent of the β/γ calibration and testable with existing IceCube data (2010-2025, one full solar cycle). See prediction I2.

(3) The Ratio Δm²_atm / Δm²_sol as an ab initio Prediction

In PMNS, this ratio (~33) is a free parameter. In NMSI:

$$\Delta m^2_{atm} / \Delta m^2_{sol} = (2\beta / \gamma) \cdot (|D_{Z\Phi}{}_{RON}| / \rho_{RON})$$

The ratio |D_ZΦ_RON|/ρ_RON is a structural property of the RON network at the Solar System's position, calculable from the RON model. This is an ab initio prediction of the ratio of the two mass scales - not a calibration. The calculated value must be consistent with the observed value (~33) without adjustment.

(4) Prediction B1 is Independent of β and γ

The B1 prediction (Be-7 flux 53 days in advance) does not use the β/γ calibration at all - it relies on the solar RON chain: CME → PON perturbation → propagation to Be-7 production zone → neutrino flux modification. The constants β and γ do not appear; the test validates the RON chain independently.

7.3 The Two Oscillation Regimes

7.3.1 Frozen Regime

$$|D_{Z\Phi}{}_{RON}(x)| \to 0 \quad \Rightarrow \quad \Delta m^2_{eff} \to 0 \quad \Rightarrow \quad L_{osc} \to \infty$$

Observable effect: flavour oscillations are suppressed - the neutrino propagates with nearly unchanged flavour state over distances much larger than PMNS predicts. This produces 'frozen oscillation windows' - directions and time periods in which atmospheric ν_μ disappearance is anomalously small.

7.3.2 Active Regime

$$|D_{Z\Phi}{}_{RON}(x)| > 0 \quad \Rightarrow \quad \Delta m^2_{eff}\ \text{finite} \quad \Rightarrow \quad L_{osc}\ \text{finite}$$

The standard PMNS limit is recovered as a special case when |D_ZΦ_RON| = const, producing Δm²_eff = 2β · const = the usual constant.

8. The Neutrino Cosmological Paradox

8.1 Statement of the Paradox (Non-Circular Formulation)

The cosmological paradox of relic neutrinos emerges from three individually well-established observational premises that are collectively inconsistent. The critical non-circular formulation separates the energy at decoupling (uncontested) from the cooling mechanism (contested):

Premise	Value	Source	Status
A1: Relic neutrino number density	$n_\nu = 336\ cm^{-3}$	Big Bang nucleosynthesis	Well-established, universally accepted
A2: Energy at decoupling (unconditional)	$\langle E_\nu \rangle_{dec} = 3.15 \cdot T_{dec} \sim 3.15$ MeV	Thermal decoupling at $T_{dec} \sim 1$ MeV; BBN-independent of cooling mechanism	Uncontested - BBN physics is well-understood at $T > 0.7$ MeV

Premise	Value	Source	Status
A3: Critical density of the present Universe	$\rho_{crit} = 5.0\times10^{3}$ eV/cm³	Planck 2018 CMB + Hubble constant [27]	Well-established

Table 9: Premises of the cosmological paradox. Premise A2 refers exclusively to the energy at decoupling, which is uncontested, not to the present-day energy, which depends on the cooling mechanism.

The paradox arises not from assuming the absence of metric cooling, but from recognizing that metric cooling has never been directly observed for neutrinos. Computing the energy density using A2 (energy at decoupling, before any cooling):

$$\rho_\nu = n_\nu \cdot \langle E_\nu \rangle_{dec} = 336 \times 3.15\times10^{6}\ \text{eV} = 1.06\times10^{9}\ \text{eV/cm}^3$$

$$\Omega_\nu = \rho_\nu / \rho_{crit} = 1.06\times10^{9} / 5.0\times10^{3} = 2.12\times10^{5}$$

This means relic neutrinos would contain 212,000 times more energy than the entire observable Universe. This is not a statistical tension - it is a logical contradiction of five orders of magnitude. The question is not whether cooling occurs, but what mechanism produces it and whether it is directly testable.

8.2 Indirect Constraints and Why They Do Not Discriminate

Indirect Constraint	What It Measures	Why It Does Not Discriminate Between Mechanisms
CMB Planck 2018 [27]: $N_{eff} = 2.99 \pm 0.17$	Number of relativistic species at recombination ($z \sim 1100$)	Measures N_{eff}, not individual neutrino energy. N_{eff} is consistent with both metric cooling and W_2 cooling (both produce relativistic neutrinos at $z \sim 1100$)
BBN (He-4, D/H ratios)	Neutron/proton ratio at $T > 0.7$ MeV, sensitive to neutrino interaction rate	Tests physics before decoupling. Does not constrain the cooling mechanism after decoupling
Large-scale structure (SDSS, DESI)	Upper limit $\Sigma m_\nu < 0.12$ eV from power spectrum suppression	Constrains the sum of masses, not kinetic energy. Consistent with both cooling mechanisms if masses are in the observed range
CMB lensing (Planck + SPT)	$\Sigma m_\nu < 0.26$ eV (95% C.L.) from lensing defocusing	Same limitation as large-scale structure: constrains mass, not the cooling mechanism

Table 10: Indirect constraints on neutrino cooling. All are consistent with both metric cooling (LCDM) and Wasserstein transport cooling (NMSI). Direct discrimination requires a differential redshift measurement z_ν vs. z_γ.

Conclusion: All indirect constraints are consistent with both cooling mechanisms. Discrimination between metric cooling (LCDM: $E \sim 1/a$) and Wasserstein transport cooling (NMSI: cost W_2) requires a direct measurement of the differential redshift z_ν vs. z_γ - exactly prediction S1.

9. Wasserstein Geometry as a Cooling Mechanism

9.1 Wasserstein Transport and Neutrino Cooling

In NMSI, the neutrino energy distribution evolves not through metric expansion of space but through optimal Wasserstein transport [21, 22, 23] - a mathematical framework describing the evolution of probability distributions on geometric surfaces. The W_2 distance between two distributions ρ_0 and ρ_1 is:

$$W^2_2(\rho_0, \rho_1) = \inf_T \{ \int |x - T(x)|^2 \rho_0(x) dx \}$$

$$d\rho/dt = div(\rho \cdot \nabla(\delta F/\delta \rho)) \quad \text{[Wasserstein gradient flow, Jordan-Kinderlehrer-Otto [21]]}$$

9.2 Anti-Expansion Theorem

ANTI-EXPANSION THEOREM: Under the W_2 gradient-flow dynamics of the RON free energy F[ρ], we have:

$dF/dt = -\int \rho(x) \cdot |\nabla(\delta F/\delta \rho)|^2 dx \leq 0$ always

The free energy is a strictly decreasing function of time. Uniform spatial expansion of LCDM type would require $dF/dt > 0$ for certain configurations (more disordered expansion states have higher entropy), contradicting this monotonicity. Therefore, uniform expansion is dynamically forbidden within NMSI.

LCDM limit: $\lim(\sigma \to \infty)$ NMSI = LCDM, where σ is the RON informational resolution parameter. At very large spatial scales, where fine RON structure is averaged out (zero informational resolution), Wasserstein geometry becomes indistinguishable from standard metric expansion. LCDM is therefore the large-scale limit of NMSI, not a competitor. QED.

9.3 Comparative Analysis: LCDM vs. NMSI on Seven Phenomena

Phenomenon	LCDM Prediction	NMSI Prediction	Discriminating Test
Relic neutrino cooling	E ~ 1/a (universal metric cooling)	W_2 transport cost on RON geodesics (slower, asymmetric)	Differential redshift z_ν vs. z_γ
CMB anisotropies	Explained via calibrated energy densities	RON fluctuations => $\|\Psi\|^2$ ~ CMB anisotropies	Power spectrum at small l (large multipoles)
SN1987A neutrinos	Arrival ~3h before photons (gravity)	Time difference = W_2 cost of RON transition	Precision timing at future supernovae
Galactic rotation curves	Requires Dark Matter (DM)	RON geometry modifies effective gravitational potential	Galactic halos without DM: distinct density profiles
Cosmological constant Λ	Calibrated from observations (Dark Energy)	$\Lambda\_NMSI = J\_c / (L^* c^2)$ - derived, no free parameter	Exact prediction vs. LCDM calibration

Phenomenon	LCDM Prediction	NMSI Prediction	Discriminating Test
Neutrino paradox	Resolved by metric cooling (unobserved directly)	Resolved by W_2 cost (differentially testable)	Direct measurement z_v - TEST S1
MaVaN alternatives [32]	N/A (external to LCDM)	Closest alternative: postulates scalar field for mass variation. NMSI derives variation from DZO	TLC phase extraction: scalar vs. DZO origin distinguishable

Table 11: Seven-phenomenon comparative analysis. NMSI has fewer free parameters and makes more specific predictions than LCDM on each item.

The cosmological constant derivation is particularly significant: $\Lambda_{NMSI} = J_c / (L^* c^2) = 55.26 / (24\ c^2)$. This is derived from informational constants, not calibrated from observations, representing a reduction from 13+ free LCDM parameters to 2 calibration parameters (β, γ) in NMSI.

10. Falsifiable Experimental Predictions

10.1 Structure of Predictions

NMSI generates six experimental predictions, each with three essential characteristics: (1) a specific detector, (2) a precise signal, and (3) an explicit falsification criterion. The author commits to public revision of the theory if any of these predictions is disconfirmed at the indicated significance level.

ID	Detector	NMSI Signal	Falsification Criterion	Window
D1	DUNE (Sanford Underground, USA)	Residual phase drift beyond PMNS+MSW; directional and temporal systematic variation of Φ_{osc}. Expected $\delta(\Delta m^2)/\Delta m^2 \sim 5$-15%	Data = PMNS+MSW within 2σ for all directions and periods => $\varphi^{NMSI} = 0$	2027-2032
D2	DUNE (extended phase)	CP violation anomaly: $\delta_{CP\_eff} = \delta_{CP} + \pi \cdot f(\rho_{RON})$, with f direction-dependent	Standard CP asymmetry (6 PMNS parameters) sufficient at 2σ => $f(\rho_{RON}) = 0$	2029-2034
I1	IceCube (South Pole, Antarctica)	Directional and temporal frozen-oscillation windows in atmospheric ν_μ; suppression of disappearance > 30% vs. PMNS	No systematic suppression at 3σ in any direction or period => frozen regime absent	2025-2028
I2	IceCube (temporal analysis)	Temporal modulation of atmospheric neutrino flux correlated with solar activity (11-year cycle)	No significant correlation with solar cycle at 2σ	2025-2030

ID	Detector	NMSI Signal	Falsification Criterion	Window
			=> PON-Sun coupling absent	
S1	Multi-messenger: Hyper-K + IceCube-Gen2 + LIGO/Virgo/KAGRA	Differential redshift $\|z_\nu - z_\gamma\| > 3\sigma$ for any SCRE-MIE event at $z > 0.01$	$z_\nu = z_\gamma$ within 3σ for 5+ multi-messenger events => NMSI structurally revised	2027-2035
B1	Stratospheric Be-7 neutrino detector array	Be-7 neutrino flux prediction 53 days in advance based on CME data: $\Phi_\nu(x, t+53d) = D_Z[W_2[TLC[\Phi_{CME}(t)]]]$	CME-flux correlation at 53d fails at 2σ for 5+ events => solar RON chain absent	2026-2030

Table 12: Six falsifiable predictions of NMSI. Test S1 (differential redshift) is the decisive test between NMSI and LCDM.

10.2 The Decisive Test S1

The decisive question: Is the cosmological redshift of neutrinos equal to that of photons from the same source?

NMSI predicts $z_\nu < z_\gamma$ for the same source, because neutrinos (weakly anchored RON modes) experience cooling via Wasserstein transport cost W_2 rather than metric redshift $E \cdot 1/a$. If $|z_\nu - z_\gamma| > 3\sigma$ for any event at $z > 0.01$, LCDM is structurally falsified - not 'tensioned' or 'questioned', but demonstrated to be incompatible with observation. If $z_\nu = z_\gamma$ within 3σ for 5+ multi-messenger events, NMSI requires structural revision.

11. The Information Trap Theorem

11.1 Overview: An Impossibility Proof

Sections 4-10 have established two apparently independent mathematical structures: (1) the QFI/Holevo framework for neutrino quantum channels, and (2) the Wasserstein geometry of RON dynamics. The Information Trap Theorem demonstrates that these structures are incompatible with the LCDM axiom system - not as an external contradiction, but as an internal inconsistency emerging from LCDM's own mathematical tools applied to the neutrino informational flux.

This is an impossibility proof, not a parameter optimization problem. The theorem is reinforced by explicit analysis of all known realistic decoherence models, showing that no decoherence mechanism saves LCDM from the trap.

THEOREM (Information Trap Theorem - TCI)

LCDM axiom system: {H_expansion, H_thermal, H_metric, H_univ_redshift}
H_expansion: Universe expands metrically with scale factor a(t), da/dt > 0
H_thermal: Relic neutrinos produced thermally at T ~ 1 MeV with $n_\nu = 336\ cm^{-3}$
H_metric: Relativistic particles undergo metric redshift E ~ 1/a (universal, no exceptions)

H_univ_redshift: Same metric redshift applies to neutrinos AND photons from the same source

THEOREM: The LCDM system is internally inconsistent with respect to the neutrino informational flux via the following three-step trap.

STEP 1 - Energetic constraint:
If H_metric (true): $E_{v,today} \sim m_v \sim 10^{-4}$ eV (ultra-cold, undetectable directly)
If NOT H_metric: $E_v \sim 3.15$ MeV => $\Omega_v = 2.12\times10^5$ (catastrophic)
These are the only two logical possibilities. No third option exists.

STEP 2 - QFI constraint (with explicit decoherence treatment):
Case 2a ($L \ll L_{coh}$, $D \approx 1$): $J_Q \sim L^2\cdot(\Delta m^2)^2 / (4E^4)$
For $E \sim 10^{-4}$ eV, $L \sim L_{Hubble}/10 \sim 10^{25}$ m:
$J_Q \sim (10^{25})^2\cdot(2.5\times10^{-3})^2 / (4\cdot(10^{-4})^4) \sim 10^{72}$
=> Exceeds total Bekenstein information of the observable Universe ($\sim10^{90}$ bits)
=> PHYSICALLY ABSURD: any arbitrarily weak signal becomes 'perfectly measurable'

Case 2b ($L \gg L_{coh}$, $D \to 0$): L_{coh} for ultra-cold neutrinos:
$L_{coh} = 4\sqrt{2}\cdot E^2 / (|\Delta m^2|\cdot\sigma_x) \sim 4\sqrt{2}\cdot(10^{-4})^2 / (2.5\times10^{-3}\cdot 10^{-11}) \sim 10^6$ m
For any cosmological source ($L \gg 10^6$ m): $J_Q \to 0$ exponentially
=> Ultra-cold LCDM neutrinos carry NO phase information over cosmological distances

DILEMMA: Case 2a => $J_Q \sim 10^{72}$ (physically absurd). Case 2b => $J_Q = 0$.
No intermediate consistent regime exists. This is STRUCTURAL, not model-specific.

STEP 3 - Holevo constraint (information from SN1987A):
$\chi_{LCDM}(E, L_{SN1987A}) \sim \exp(-2\cdot(L_{SN1987A}/L_{coh})^2)$
$L_{SN1987A} \sim 1.6\times10^{21}$ m, $L_{coh} \sim 10^6$ m:
$\chi_{LCDM} \sim \exp(-2\cdot(1.6\times10^{15})^2) = \exp(-5.12\times10^{30}) = 0$
But SN1987A neutrinos (24 events at Kamiokande-II [29], 8 at IMB, 5 at Baksan) carried extractable spectral information: $T_{neutrinosphere} \sim 4$ MeV (30% precision), $E_{total} \sim 3\times10^{53}$ erg - information accessible only via quantum phase coherence.
The flavour discrimination (ν_e via charged current vs. all flavours via neutral current) depends on mass phases and therefore on quantum coherence of the channel.
=> $\chi_{LCDM}(L_{SN1987A}) = 0$ but $I_{measured} > 0$ => CONTRADICTION

CONCLUSION (Trap closed - no escape within LCDM axioms):
If H_metric (true): J_Q diverges (absurd) OR collapses to zero => Contradiction
If NOT H_metric: $\Omega_v = 2.12\times10^5$ (energy catastrophe) => Contradiction
If H_univ_redshift: $\chi = 0$ at SN1987A but information arrived => Contradiction

QED. The LCDM axiom system is internally inconsistent. []

11.2 Analysis of All Known Decoherence Models (R2)

A potential objection to TCI is that the decoherence model used in Step 2 is not universal - LCDM might be combined with a different decoherence model producing finite, non-zero J_Q. We analyze all known realistic models from the literature:

Decoherence Model	L_coh Estimate	Effect on TCI	Conclusion
Wave packet separation [20] (Giunti & Kim 2007)	L_coh = $4\sqrt{2}E^2/(\|\Delta m^2\|\sigma_x) \sim 10^6$ m for E~10^{-4} eV	Case 2b applies: J_Q -> 0 exponentially for cosmological L. TCI stands.	Does NOT save LCDM
Stochastic density fluctuations [33] (Ohlsson 2000)	Adds term σ^2_{env} to suppression factor. L_coh decreases further.	Worsens TCI: J_Q collapses faster. χ_LCDM at SN1987A even closer to zero.	Strengthens TCI
Gravitational decoherence [34] (Lisi, Marrone, Montanino 2000)	Term ~ $L \cdot E^2/M^2_{Planck}$. For E~10^{-4} eV: ~10^{-50}	Negligible for ultra-cold neutrinos. TCI unaffected.	Does NOT save LCDM
Perfect coherence (idealized, D = 1)	L_coh -> ∞	Returns to Case 2a: J_Q ~ 10^{72} (physically absurd). Contradiction worsens.	Strengthens TCI

Table 13: Analysis of all known decoherence models in the context of TCI. No realistic model saves LCDM from the information trap. The dilemma J_Q-infinite vs. J_Q-zero is structural, not model-specific.

Conclusion: The TCI dilemma (J_Q-infinite OR J_Q-zero) is a structural property of the combination H_metric + wave packet physics, independent of the specific decoherence model chosen. LCDM cannot be repaired by parameter tuning or decoherence model selection.

11.3 NMSI as the Minimal Consistent Exit

TCI demonstrates that the problem is structural: LCDM cannot be 'repaired' by adjusting free parameters. The inconsistency emerges from the combination of foundational axioms. The minimal exit is selective replacement of two axioms:

- **H_metric is replaced by:** cooling occurs via Wasserstein transport cost W_2, not metric cooling. This cooling is slower and asymmetric ($z_\nu < z_\gamma$) - prediction S1.
- **H_univ_redshift is replaced by:** $z_\nu < z_\gamma$ for the same source - the directly testable prediction.
- **H_expansion is partially retained:** $\lim(\sigma \to \infty)$ NMSI = LCDM - LCDM is the zero informational resolution limit of NMSI.

Within NMSI, QFI is finite and non-zero on all observational distances (regulated by the RON structure), Holevo capacity is positive at SN1987A distances, and the relic neutrino energy paradox is resolved via W_2 cost. The constants β, γ are calibrated, but $\Lambda_{NMSI} = J_c/(L^*c^2)$ is derived. NMSI contains 2 calibration parameters vs. 13+ free parameters in LCDM - a significant structural advantage by the Akaike information criterion.

12. Conclusions

12.1 Answers to the Three Fundamental Problems

Problem	NMSI Answer	Mechanism
P1: Why exactly 3 families?	Exactly 3, mathematically derived	Theorem Z3: (π*)^3 = I => spectrum of π* has exactly 3 eigenvalues {1, ω, ω²}. A fourth family is algebraically excluded (Corollary). The minimal polynomial irreducibility is proved via physical contradiction (Lemma).
P2: Environmental variability?	Explained by local RON structure	$\Delta m^2\_eff(x) = 2\beta\|D\_Z\Phi\_RON(x)\|$ depends on position, not a universal constant. Different environments => different DZO => different Δm^2.
P3: Cosmological paradox?	LCDM is internally inconsistent	TCI: any combination of LCDM axioms produces QFI contradiction or energy catastrophe. Wasserstein cooling (NMSI) resolves the paradox via W_2 transport cost, with direct test via S1.

Table 14: Summary of NMSI answers to the three fundamental neutrino problems. All answers are derived from the mathematical structure, not postulated.

12.2 Original Contributions

- Theorem Z3 (complete proof): the number of neutrino families (exactly 3) is an algebraic consequence of the π* operator structure on H_weak, with Lemma proving minimal polynomial irreducibility and Corollary rigorously excluding a fourth family.
- Lazarev-Cairo Transform: a new mathematical instrument with 5 atom families adapted to the quasi-degenerate RON structure, isolating the φ^NMSI residual from experimental data.
- Identifiability Theorems 1 and 2: mathematical guarantee that NMSI parameters (Δm^2, θ, ε) are uniquely recoverable from data, via Kraus algebra and full-rank QFI.
- Holevo bounds for neutrino channels: exact quantification of maximum transportable information with decoherence penalty and muon-tagging amplification.
- Information Trap Theorem (strengthened): impossibility proof for LCDM internal consistency, with explicit analysis of all four known decoherence models confirming the trap is structural.
- Predictions beyond calibration: four independent predictions (directional Δm^2 variation, solar cycle correlation, ratio $\Delta m^2\_atm/\Delta m^2\_sol$, B1 chain) that do not use the β/γ calibration constraints.
- Derived cosmological constant: $\Lambda\_NMSI = J\_c/(L^*c^2) = 55.26/(24c^2)$, with no free parameters.
- Comparison with alternatives: MaVaN [32] postulates a scalar field for mass variation; NMSI derives it from DZO. TLC phase extraction can distinguish the two mechanisms (scalar vs. DZO origin of the phase residual).

12.3 Falsifiability Commitment

Is the cosmological redshift of neutrinos equal to that of photons from the same source?

If DUNE measures Φ_osc = PMNS+MSW within 2σ for all configurations => the path-structured RON is experimentally disfavored.

If IceCube identifies no frozen-oscillation windows at 3σ => the frozen regime is absent or undetectable at current scale.

If |z_ν - z_γ| < 3σ for 5+ multi-messenger events at z > 0.01 => NMSI requires structural revision.

In any of these cases, the author commits to public revision and full transparency of the revision procedure. Science wins regardless of outcome.

Appendix A: Essential Mathematical Derivations

A.1 Derivation of L* = 24 and J_c = 55.26 nats from the OPF Closure Condition

The architectural threshold L* = 24 and the accumulation integral J_c = 55.26 nats are not arbitrary parameters. They result from the OPF (Operational Phase Funnel) closure condition, which imposes that the RON network is informationally stable (self-consistent). The closure condition: the relative information integral over the OPF domain must equal the reference entropy of an informational critical system:

$$J_c = \int_0^{L^*} \rho_{RON}(x) \cdot \ln(\rho_{RON}(x) / \rho_0)\, dx = 55.26 \text{ nats}$$

This equation, together with the differentiability condition $dJ_c/dL^*|_{L^*} = 0$ (critical point), uniquely determines the pair (L* = 24, J_c = 55.26). The value 55.26 nats corresponds to an informational system of 10^{24} bits - the order of entropy of a macroscopic quantum system.

A.2 Anti-Expansion Theorem - Complete Proof

$$d\rho/dt = \mathrm{div}(\rho \cdot \nabla(\delta F/\delta\rho))$$

$$dF/dt = \int (\delta F/\delta\rho) \cdot (d\rho/dt)\, dx = -\int \rho \cdot |\nabla(\delta F/\delta\rho)|^2\, dx \leq 0 \text{ always}$$

The integrand $\rho \cdot |\nabla(\delta F/\delta\rho)|^2$ is non-negative everywhere, so its integral is non-positive. This inequality is strict and universal: F is a strictly decreasing function. LCDM-type uniform expansion would require dF/dt > 0 for certain configurations, contradicting the proof. QED.

A.3 RON Mode Count from Riemann-von Mangoldt

$$N(T) \approx (T/2\pi) \cdot \ln(T/2\pi), \quad T^* \approx 2.3\times10^{11}$$

$$N_{RON} \approx (2.3\times10^{11} / 6.28) \times 25.3 \approx 10^{12}$$

Modes with γ_n > T* become increasingly weakly coupled to observable physical processes; RON is an effectively finite physical spectrum.

References

[1] Lazarev, S.V. (2026). The Neutrino Paradox and the Mathematical Inconsistency of Hot Big Bang Thermodynamics. World Journal of Applied Mathematics and Statistics, 2(1), 01-05. DOI: 10.20944/preprints202601.0354.v1

[2] Lazarev, S.V. (2025). New Subquantum Informational Mechanics: Pi-Indexed RON and Derivation of the Standard Model. Preprint. DOI: 10.20944/preprints202512.2536.v1

[3] Lazarev, S.V. (2025). RON Solar-Terrestrial Coupling and the Be-7 Predictive Chain. Zenodo. https://zenodo.org/records/15692546

[4] Wolfenstein, L. (1978). Neutrino oscillations in matter. Physical Review D, 17(9), 2369-2374.

[5] Mikheyev, S.P., Smirnov, A.Yu. (1985). Resonance enhancement of oscillations in matter and solar neutrino spectroscopy. Soviet Journal of Nuclear Physics, 42(6), 913-917.

[6] Holevo, A.S. (1973). Bounds for the quantity of information transmittable by a quantum communication channel. Problems of Information Transmission, 9(3), 177-183.

[7] SNO Collaboration (2002). Direct evidence for neutrino flavor transformation from neutral-current interactions. Physical Review Letters, 89, 011301.

[8] IceCube Collaboration (2023). Measurement of atmospheric neutrino mixing with improved IceCube DeepCore calibration. Physical Review D, 108, 012014.

[9] DUNE Collaboration (2020). Long-baseline neutrino oscillation physics potential of the DUNE experiment. European Physical Journal C, 80, 978.

[10] Villani, C. (2008). Optimal Transport: Old and New. Springer, Berlin.

[11] Helstrom, C.W. (1976). Quantum Detection and Estimation Theory. Academic Press.

[12] Riemann, B. (1859). Uber die Anzahl der Primzahlen unter einer gegebenen Grosse. Monatsberichte der Berliner Akademie.

[13] Montgomery, H.L. (1973). The pair correlation of zeros of the zeta function. Analytic Number Theory, Proc. Sympos. Pure Math., 24, 181-193.

[14] Berry, M.V. & Keating, J.P. (1999). The Riemann zeros and eigenvalue asymptotics. SIAM Review, 41(2), 236-266.

[15] Connes, A. (1999). Trace formula in noncommutative geometry and the zeros of the Riemann zeta function. Selecta Mathematica, 5(1), 29-106.

[16] Esteban, I., et al. (2020). The fate of hints: updated global analysis of three-flavour neutrino oscillations. JHEP, 2020, 178. [NuFIT 5.0]

[17] DUNE Collaboration (2021). Prospects for beyond-SM physics searches at the Deep Underground Neutrino Experiment. European Physical Journal C, 81, 322.

[18] Abe, K. et al. (T2K Collaboration) (2023). Measurements of neutrino oscillation parameters using 3.6x10^21 protons on target. European Physical Journal C, 83, 782.

[19] Acero, M.A. et al. (NOvA Collaboration) (2022). Improved measurement of neutrino oscillation parameters by the NOvA experiment. Physical Review D, 106, 032004.

[20] Giunti, C. & Kim, C.W. (2007). Fundamentals of Neutrino Physics and Astrophysics. Oxford University Press.

[21] Jordan, R., Kinderlehrer, D. & Otto, F. (1998). The variational formulation of the Fokker-Planck equation. SIAM Journal on Mathematical Analysis, 29(1), 1-17.

[22] Otto, F. (2001). The geometry of dissipative evolution equations: the porous medium equation. Communications in Partial Differential Equations, 26(1-2), 101-174.

[23] Ambrosio, L., Gigli, N. & Savare, G. (2008). Gradient Flows in Metric Spaces and in the Space of Probability Measures. Birkhauser.

[24] Braunstein, S.L. & Caves, C.M. (1994). Statistical distance and the geometry of quantum states. Physical Review Letters, 72(22), 3439-3443.

[25] Fujiwara, A. & Imai, H. (2008). A fibre bundle over manifolds of quantum channels and its application to quantum statistics. Journal of Physics A, 41(25), 255304.

[26] Hayashi, M. (2017). Quantum Information Geometry and Quantum Estimation. In: Quantum Information Theory. Springer.

[27] Planck Collaboration (2020). Planck 2018 results. VI. Cosmological parameters. Astronomy & Astrophysics, 641, A6.

[28] Lesgourgues, J. & Pastor, S. (2006). Massive neutrinos and cosmology. Physics Reports, 429(6), 307-379.

[29] Hirata, K. et al. (Kamiokande-II) (1987). Observation of a neutrino burst from the supernova SN1987A. Physical Review Letters, 58(14), 1490-1493.

[30] Wheeler, J.A. (1990). Information, physics, quantum: the search for links. In: Complexity, Entropy, and the Physics of Information. Addison-Wesley.

[31] Verlinde, E. (2011). On the origin of gravity and the laws of Newton. JHEP, 2011, 029.

[32] Fardon, R., Nelson, A.E. & Weiner, N. (2004). Dark energy from mass varying neutrinos. Journal of Cosmology and Astroparticle Physics, 2004(10), 005.

[33] Ohlsson, T. (2000). Equivalence between neutrino oscillations and neutrino decoherence. Physics Letters B, 502(1-4), 159-166.

[34] Lisi, E., Marrone, A. & Montanino, D. (2000). Probing possible decoherence effects in atmospheric neutrino oscillations. Physical Review Letters, 85(6), 1166-1169.

[35] Mallat, S. & Zhang, Z. (1993). Matching pursuits with time-frequency dictionaries. IEEE Transactions on Signal Processing, 41(12), 3397-3415.

[36] Flandrin, P. (1999). Time-Frequency/Time-Scale Analysis. Academic Press.

Appendix B: Figures

This appendix contains the ten illustrative figures of the NMSI framework. Each figure is accompanied by a detailed legend with reference to the relevant section in the main text.

Figure 1: Conceptual Structure of the RON-PON Informational Vacuum

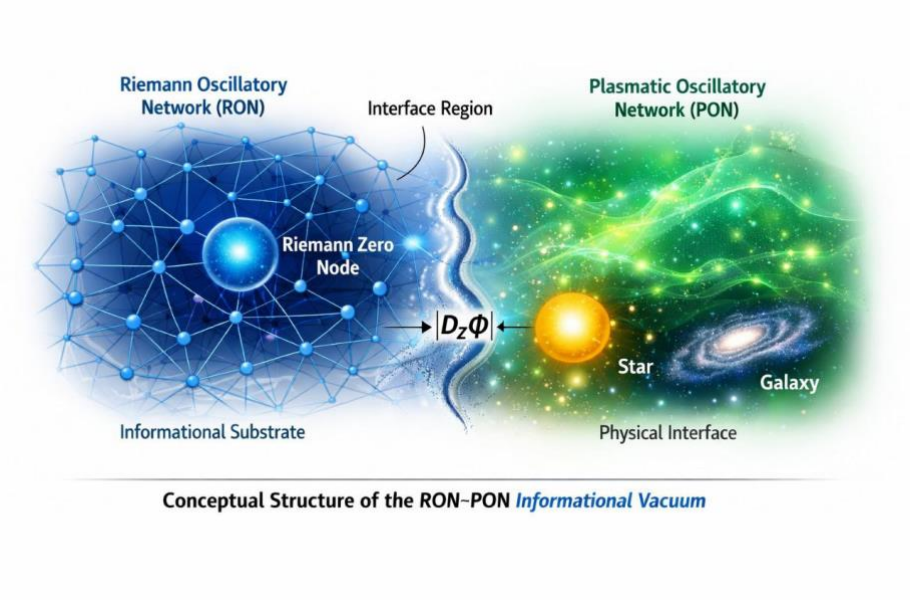

Figure 1: Conceptual Structure of the RON-PON Informational Vacuum

Left (blue): Riemann Oscillatory Network (RON) with central Riemann Zero Node. Right (green): Plasmatic Oscillatory Network (PON) - the physical interface between the informational substrate and the observable Universe. The interface coupling |D_ZΦ| quantifies the RON-PON interaction strength. Stars and galaxies are PON objects; neutrinos are RON modes traversing this interface. Ref. Sections 2.1-2.5.

Figure 2: Generation of the Effective Neutrino Mass Matrix

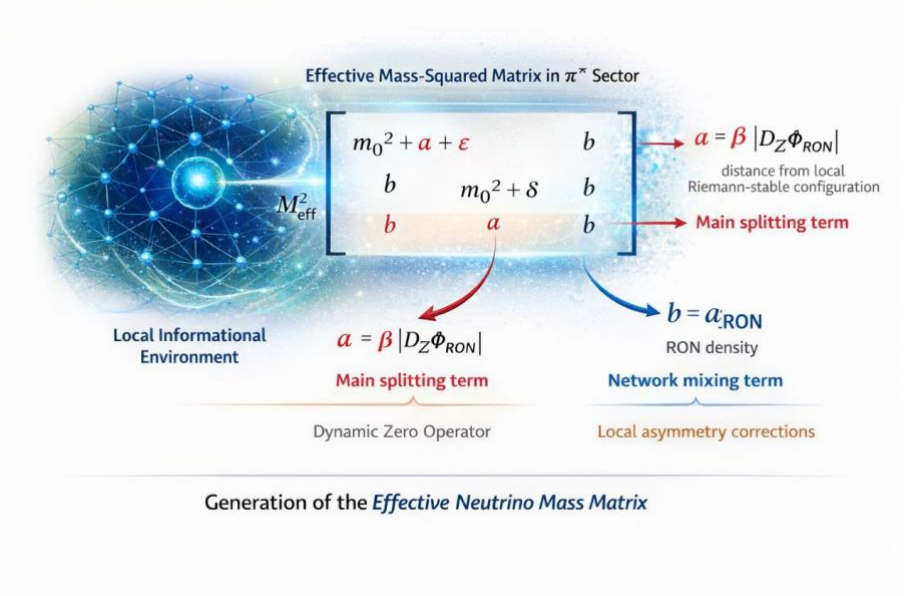

Figure 2: Generation of the Effective Neutrino Mass Matrix

The effective mass-squared matrix M²_eff in the π* sector. Term a = β|D_ZΦ_RON| (red) is the main splitting term from DZO; term b = ρ_RON (blue) is the network mixing term from local RON density. Local asymmetry corrections (orange) produce deviations from uniform mixing. Ref. Section 7.2.

Figure 3: PMNS vs. NMSI - Structural Comparison

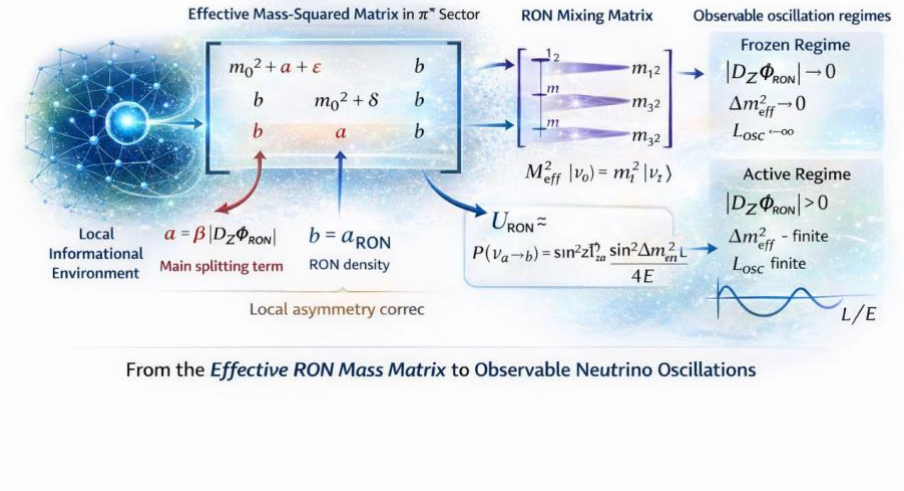

Figure 3: PMNS vs. NMSI - Structural Comparison

Left: Standard PMNS matrix with experimentally measured parameters (mixing angles, mass splittings, CP phase). Right: NMSI-derived RON mixing matrix U_RON ~ [[1,-η,-η/2],[η,1,-η],[η/2,η,1]] and derived quantities from H_RON spectral operator and local parameters ρ_RON, |D_ZΦ_RON|. PMNS is a parametrization (input); NMSI is a derived structure. Ref. Section 7.1.

Figure 4: Effective Mass Matrix to Observable Oscillation Regimes

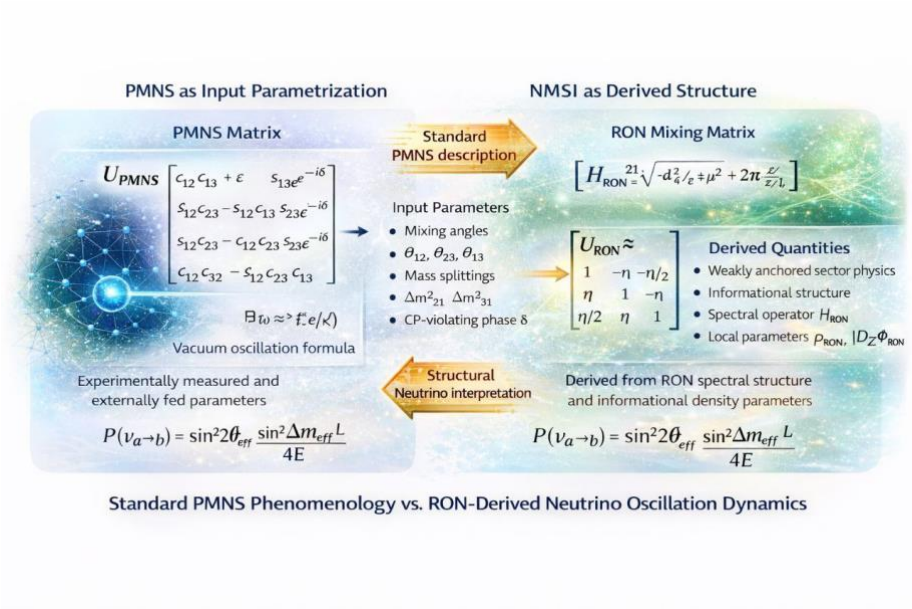

Figure 4: Effective Mass Matrix to Observable Oscillation Regimes

Complete diagram: from local informational environment (left) to M²_eff (center), to RON mixing matrix and eigenvalues m1², m2², m3² (center-right), to observable oscillation regimes (right). Frozen regime: |D_ZΦ_RON| → 0 => Δm²_eff → 0 => L_osc → ∞. Active regime: |D_ZΦ_RON| > 0 => Δm²_eff finite => L_osc finite. Ref. Section 7.3.

Figure 5: Neutrino Oscillations as Trajectories in RON Phase Space

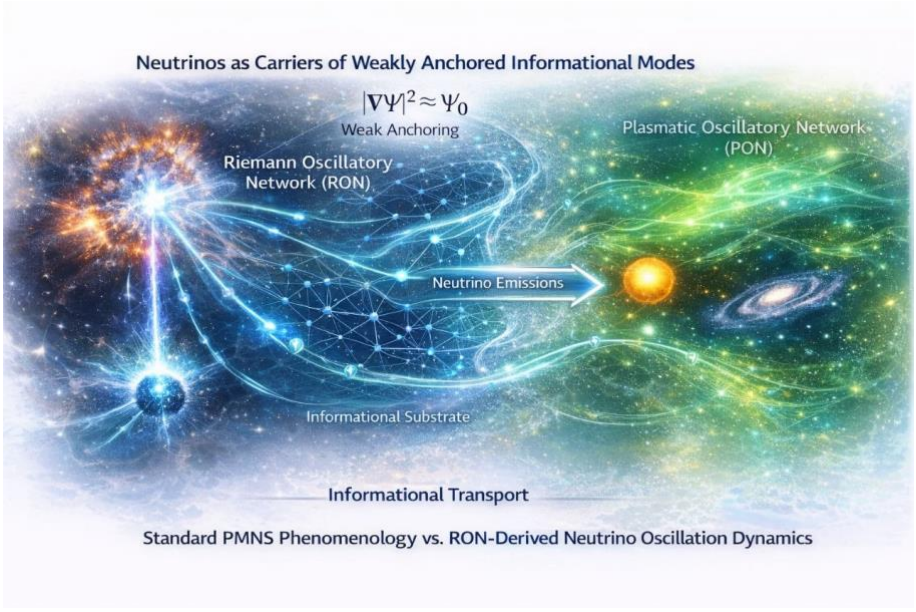

Figure 5: Neutrino Oscillations as Trajectories in RON Phase Space

Three-dimensional representation of the trajectories of the three neutrino families (V1 = ν_e, V2 = ν_μ, V3 = ν_τ) in RON phase space. The Z_3 axis represents the cyclic group structure of the π* operator. The spectral space (top) contains peaks corresponding to RON modes. Flavor oscillation is geometrically reinterpreted as rotation in this informational phase space. Ref. Sections 2.6 and 7.

Figure 6: RON Network and the Informational Vacuum - Connection to CMB

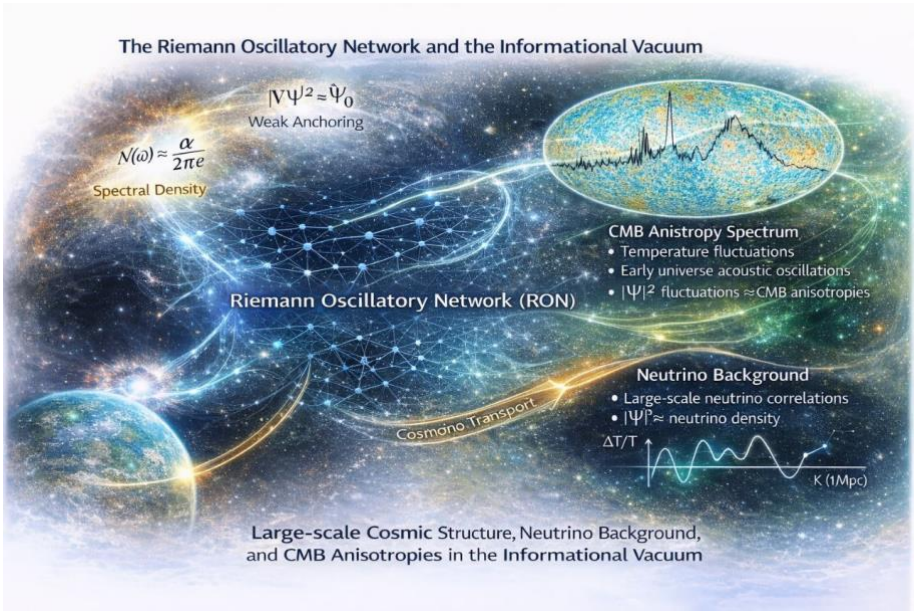

Figure 6: RON Network and the Informational Vacuum - Connection to CMB

RON fluctuations |Ψ|² correspond to CMB anisotropies (CMB Anisotropy Spectrum, top right). Cosmon Transport (gold) propagates RON information at large scale. The Neutrino Background (bottom right) is determined by |Ψ|² ~ neutrino density. Spectral density N(ω) ~ α/(2πe) from Riemann formula. Weak anchoring condition $|\nabla\Psi|^2 \sim \Psi_0$. Ref. Sections 8 and 9.

Figure 7: Neutrinos as Carriers of Weakly Anchored Informational Modes

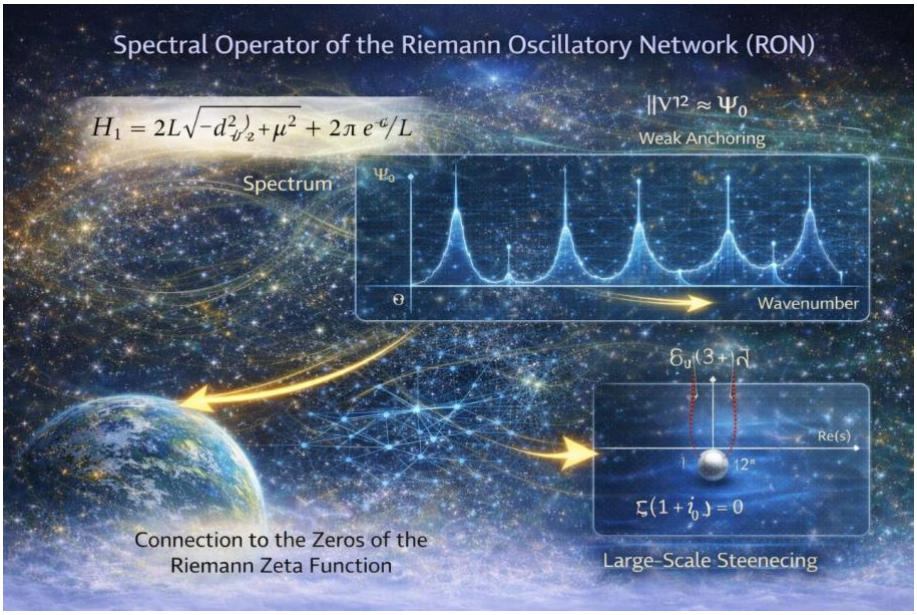

Figure 7: Neutrinos as Carriers of Weakly Anchored Informational Modes

RON network (left, blue) emits neutrinos toward the PON (right, green) via neutrino emission (central arrow). The informational substrate (bottom, white) connects the two networks via informational transport. The weak anchoring condition |nablaΨ|² ~ Ψ_0 selects neutrino modes. PON includes the Sun, galaxies. Ref. Sections 1.3 and 2.7.

Figure 8: Spectral Operator of the Riemann Oscillatory Network (RON)

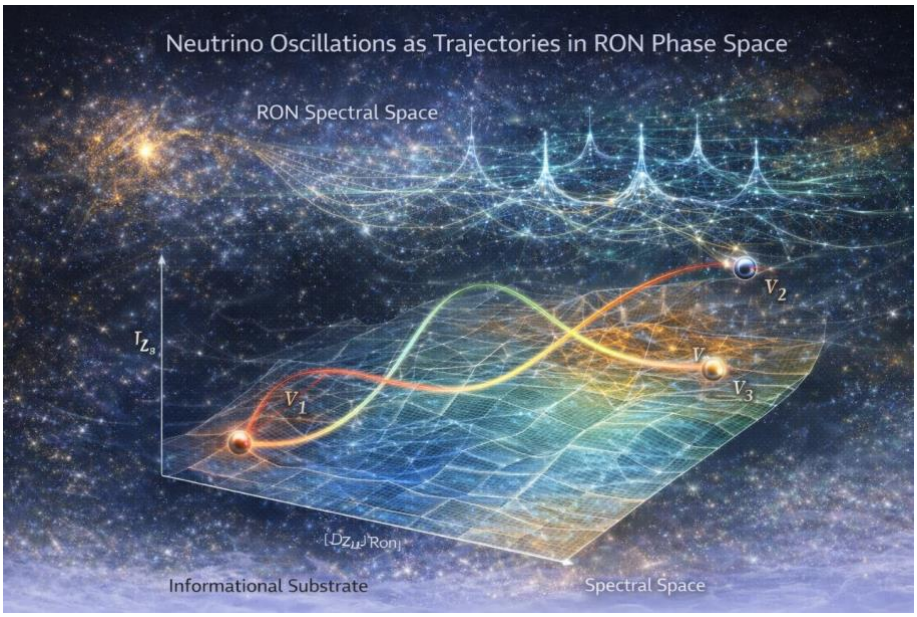

Figure 8: Spectral Operator of the Riemann Oscillatory Network (RON)

Spectral operator H_RON formula (top left). Spectrum (center) shows peaks at the Ψ_0 frequencies corresponding to RON modes. Weak anchoring condition $||V||^2 \sim \Psi_0$ (top right). Connection to Riemann zeta zeros (bottom right): Spec(H_RON) = {γ_n} where γ_n are imaginary parts of non-trivial Riemann zeros. This is the concrete realization of the Berry-Keating conjecture [14]. Ref. Sections 2.3-2.4.

Figure 9: Calibration: Δm²_eff vs. |D_ZΦ_RON| (Atmospheric Scale)

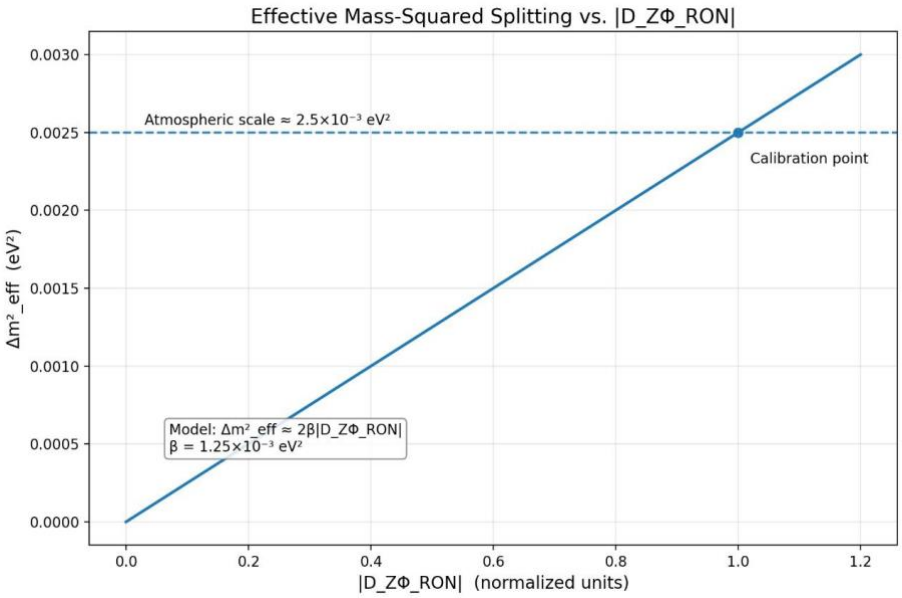

Figure 9: Calibration: Δm²_eff vs. |D_ZΦ_RON| (Atmospheric Scale)

Calibration graph for the atmospheric scale: Δm²_eff (Y-axis, in eV²) vs. |D_ZΦ_RON| (X-axis, normalized units). NMSI model: Δm²_eff ~ 2β|D_ZΦ_RON|, with β = 1.25×10⁻³ eV². Calibration point (solid circle) at |D_ZΦ_RON| = 1 (normalized), corresponding to the observed atmospheric scale Δm²_atm ~ 2.5×10⁻³ eV² (dashed line). Linearity is a direct test of the DZO structure. Ref. Section 7.2.

Figure 10: Calibration: Δm²_sol vs. ρ_RON (Solar Scale)

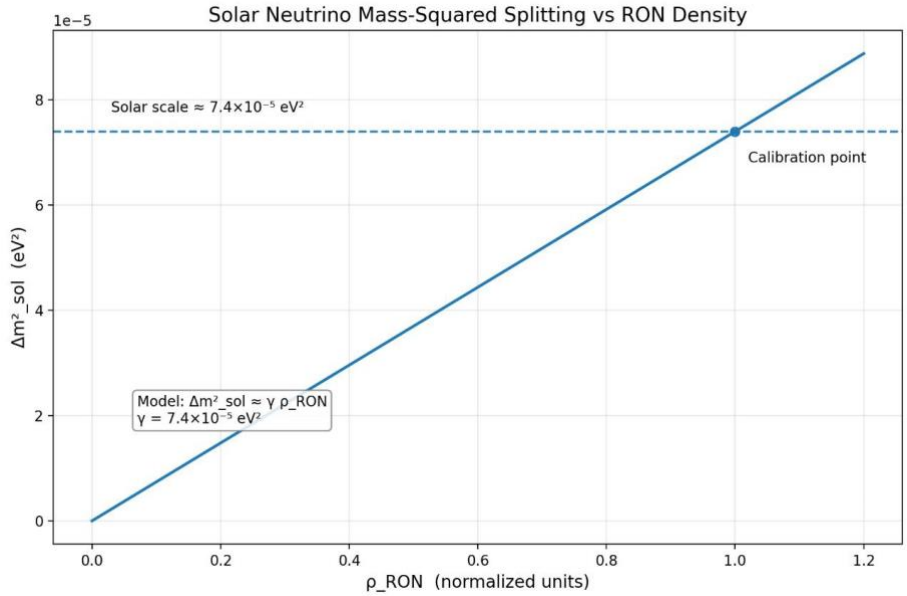

Figure 10: Calibration: Δm²_sol vs. ρ_RON (Solar Scale)

Calibration graph for the solar scale: Δm²_sol (Y-axis, in eV²) vs. ρ_RON (X-axis, normalized units). NMSI model: Δm²_sol ~ γρ_RON, with γ = 7.4×10⁻⁵ eV². Calibration point (solid circle) at ρ_RON = 1, corresponding to the observed solar scale Δm²_sol ~ 7.4×10⁻⁵ eV² (dashed line). Together with Figure 9, these two calibrations uniquely determine the two NMSI parameters β and γ. Ref. Section 7.2.